Application of post-consumer recycled high-impact polystyrene in the preparation of phase-inversion membranes for low-pressure membrane processes

Jorge Garcia-Ivars*[a], Xin Wang-Xu[b], Maria-Isabel Iborra-Clar[a,c]

[a]Research Institute for Industrial, Radiophysical and Environmental Safety (ISIRYM), Universitat Politècnica de València, C/Camino de Vera s/n, 46022 Valencia, Spain

[b]School of Industrial Engineering (ETSII), Universitat Politècnica de València, C/Camino de Vera s/n, 46022 Valencia, Spain

[c]Department of Chemical and Nuclear Engineering, Universitat Politècnica de València, C/Camino de Vera s/n, 46022 Valencia, Spain

Tel. +34 963879633

Fax. +34 963877639

Correspondence to: Jorge Garcia-Ivars (E-mail: *jorgariv@posgrado.upv.es*)

ABSTRACT

In this study, recycled plastic waste was successfully used in preparing low-pressure membranes by phase-inversion method. These membranes are considered as an alternative solution for economical and environmental concerns, namely: water reclamation as well as polymer recycling and reuse. Post-consumer recycled high-impact polystyrene and virgin commercial high-impact polystyrene were separately used to prepare membranes, which were thereafter compared in terms of their respective characteristics and performance. N,N-Dimethylacetamide and deionised water were used as a solvent and coagulant, respectively. Membranes were characterised by microscopic observations, contact angle measurements, thermogravimetric analysis, and filtration experiments. The recycled polymeric membranes presented similar thermal properties as the membranes made from commercial high-impact polystyrene, which were used as control membranes. They also obtained similar asymmetric membrane structures, however with slightly higher porosity (from 47.54 ± 5.53 % for control membranes to 52.31 ± 4.33 % for recycled polymeric membranes). The presence of additives in the recycled polymeric structure was confirmed by EDX results. Such additives made the membranes to become more hydrophilic, reducing the water contact angle value from 81.78 ± 3.42 º obtained for control membranes to 79.19 ± 4.15 º. Moreover, irreversible fouling was satisfactorily minimised and humic acid rejection was very slightly enhanced (from 95.5 ± 0.2 to 96 ± 0.1 %). This indicates that the more hydrophilic the membrane is, the better antifouling properties it possesses. Thus, the results of the post-consumer recycled high-impact polystyrene suggest that they can provide a sustainable and environmental alternative when implemented in low-pressure membrane processes.

KEYWORDS Recycled plastic waste; High-impact polystyrene; Low-pressure membrane filtration systems; Antifouling properties; Membrane characterisation.

1. INTRODUCTION

Water scarcity is a serious environmental concern that affects the natural environment, wildlife and mankind due to the fact that water (especially freshwater) is the most fundamental natural resource for the development and survival of living organisms in the world [1]. Nowadays, the increasing environmental problems related to both climate change and human socioeconomic development have irretrievably modified the dynamic water cycle, which led to the degradation of ground and surface waters (affecting both health and biodiversity of aquatic and terrestrial environments) and therefore brought about a dangerous imbalance between demand and limited availability of freshwater [1-3]. It is very important to keep in mind that water is an unalienable individual and collective right for every living organism [4]. Therefore, the enormity of such problems obliges researchers to search for solutions and to implement sustainable and "clean" technologies and resources, which is significant in the 21th century. Treatment, reclamation and reuse of wastewater in a cost-effective manner would render wastewater a sustainable water resource that could help to alleviate the water shortage [5].

Currently, there is a growing concern over the environmental impact of the ever increasing use of plastic and the associated generation of plastic waste, particularly non-biodegradable and toxic by-products, which also present disposal challenges at the landfill [6]. Polymers are produced using petroleum as their principal feedstock and are one of the most widely used materials for several applications for industrial, agricultural and household activities, mainly due to their good mechanical properties, versatility, low density and ease of processing. Like freshwater and other natural resources, petroleum is becoming scarcer and more expensive. As a result, new alternative sources with less environmental impact as well as more clean technologies should be considered for plastic production. In this regard, feasible sources could be biomass and natural gas; however they are currently not economic alternatives. Among the different ways to deal with plastic waste (which include combustion and burying underground, which are unfriendly environmental processes due to the formation of toxic gases and fumes as well as the pollution of surface and ground waters), plastic recycling is therefore often the best environmental approach and could be considered as an area of particular interest, especially for reducing the need to produce new plastics as well as other polymer based products [6,7]. Among the different plastics that can be recycled include polyethylene terephthalate (PET), polyvinyl chloride (PVC), polypropylene (PP) or high-density polyethylene (HDPE), these plastics are having different identification codes and they have been used in a wide range of applications, such as packaging, appliances, automotive components, toys, and electrical and electronic equipment. High-impact polystyrene is a multiphase copolymer system which is formed by polybutadiene rubber particles dispersed in a matrix structure of polystyrene [8]. Its main advantages include good impact resistance, ease of moulding and processing, stability and low cost.

In this work, membranes were developed via phase-inversion method from post-consumer high-impact polystyrene. The aim was to assess the feasibility of using recycled plastic material to prepare membranes which could be applied in microfiltration and ultrafiltration processes. The novelty of this study lies in the use of post-consumer high-impact polystyrene for preparing membranes which could be used for different water applications such as water reclamation, thus promising to provide environmental and economic benefits in a way.

2. EXPERIMENTAL

2.1. Chemicals and Materials

Commercial high-impact polystyrene (HIPS, Polystyrol 476L, supplied by BASF Co., Germany) and recycled high-impact polystyrene (HIPS-R, supplied by Acteco S.L., Spain) were used as base polymers and N,N-Dimethylacetamide (DMA) was employed as a solvent. The non-woven support was commercial grade Viledon FO 2431 (Freudenberg, Germany). Humic acid (HA) solutions with concentration of 50 mg/L (at pH 7) were used as common model foulants to study the antifouling ability of the synthesised membranes due to the fact that HA can be considered as the main component of the natural organic matter (NOM) present in surface and ground waters. Both DMA and HA were purchased from Sigma-Aldrich (Germany). The pH of feed solutions was adjusted using 0.1 M NaOH (Panreac, Spain). Deionised water was used throughout this study. Solvents and chemicals were used without further purification.

2.2. Membrane preparation

Membranes were prepared from homogeneous polymeric solutions (from HIPS and HIPS-R, separately) in DMA by the non-solvent induced phase separation method (NIPS). The composition of both polystyrene/DMA solutions was 20/80 wt%. Such solutions were prepared under mechanical stirring at room temperature (20 ºC) for at least 48 h until a homogeneous solution was obtained and thereafter, were put into a vacuum oven to remove the air bubbles trapped (50 ºC, 15 min). The polymeric solutions were uniformly cast onto non-woven supports using a film applicator (K101 Automatic Film Applicator, RK Print-Coat Instruments Ltd, UK) with a 100 µm casting knife at room temperature and controlled relative humidity (40%). They were immersed in a coagulation bath (distilled water at a temperature between 10 and 15 ºC) for 30 min to complete the phase separation. After the precipitation, the membranes were washed in order to remove residual solvent and were kept in deionised water for further testing.

2.3. Cloud point measurements

The ternary phase diagrams for HIPS/DMA/water systems were constructed by cloud point measurements using the titration method described in a previous work [9]. The function of a phase diagram is to describe the phase behaviour of a polymer-solvent mixture and its possible phase separation, which leads to different membrane morphology and structure: symmetrical non-porous membrane, symmetrical porous membrane, and asymmetric membrane formed by a thin dense top layer on a porous substructure [10].

2.4. Viscosity measurements

The viscosity of the different polymeric solutions was measured by a Brookfield digital viscometer (Model DVII+, United States of America) at 20 ºC.

2.5. Membrane characterisation

High-impact polystyrene membranes were characterised in terms of morphology, hydrophilicity, and permeation properties. Morphology and composition were analysed by Fourier transform infrared-attenuated total reflection (FTIR-ATR), scanning electron microscopy (SEM), atomic force microscopy (AFM), thermogravimetric analysis (TGA), and energy dispersive X-ray spectroscopy (EDX). Hydrophilicity was also evaluated using porosity (ε), equilibrium water content (EWC) and contact angle measurements. Finally, permeation properties were tested by water permeation (obtaining the hydraulic permeability of each membrane) and humic acid rejection.

Cross-sectional morphologies of the membranes were observed using a scanning electron microscope (JEOL JSM6300, Japan) equipped with an EDX spectrometer. Samples were dried overnight and fractured in liquid nitrogen. After that, membrane samples were sputtered with a thin conductive layer of carbon before SEM analysis. EDX results provided the real composition of the measured area on the membrane surface and were averaged from ten different locations for each sample.

A multimode atomic force microscope (VEECO Instruments, USA) was used to record images of the membrane surfaces in ambient air by tapping mode. The AFM images were acquired at a scan size of 1 µm x 1 µm. Surface roughness was evaluated using the mean roughness parameter (S_a) by averaging the roughness values obtained from random 1 µm x 1 µm areas of each membrane sample:

$$S_a = \frac{1}{N}\sum_{i=0}^{N}\left|Z_i - Z_{avg}\right| \qquad \text{Eq. (1)}$$

where Z_i is the current Z value measured, Z_{avg} is the average of the different Z values within the given area, and N is the number of data points considered (512 data points).

FTIR-ATR analysis was performed in order to evaluate the differences between the chemical structures of the different membranes. FTIR-ATR spectra were measured on a Perkin-Elmer Spectrum 100 spectrometer equipped with an HATR accessory consisting of a ZnSe crystal at a nominal incident angle of 45 º. For each measurement, 64 scans were performed for an operating range from 400 to 4000 cm^{-1} with a resolution of 4 cm^{-1}. Before FTIR-ATR analysis, samples were dried in a desiccator overnight at room temperature.

The thermal stability of the membranes was evaluated by thermogravimetric analysis (TGA) using a TGA-DSC thermobalance (Perkin Elmer DSC 8000, USA). It was operated at the heating ramp of 10 ºC/min from 30 ºC to 900 ºC under nitrogen gas with a flow of 50 mL/min.

In order to assess the surface hydrophilicity of the membranes, porosity, equilibrium water content (EWC) and water contact angle of each membrane were studied. Average porosity (ε) was determined by wet-dry weighting method, where the wet weight (W_W) was measured at wet state after wiping the excess water on the sample surface while the dry weight (W_D) was obtained after drying such samples in a vacuum oven for 24 h at 50 °C. Thus, both parameters (ε and EWC) were calculated using the following equations:

$$\varepsilon(\%) = \frac{\frac{(W_W - W_D)}{\rho_W}}{\frac{(W_W - W_D)}{\rho_W} + \frac{W_D}{\rho_p}} \cdot 100 \qquad \text{Eq. (2)}$$

$$EWC(\%) = \frac{W_W - W_D}{W_W} \cdot 100 \qquad \text{Eq. (3)}$$

where W_W and W_D are the wet and dry weight of the membrane (g), respectively; ρ_w is the density of water at operating conditions (g/cm^3) and ρ_p is the density of the corresponding polymer (g/cm^3).

Water contact angles were measured using the sessile drop method with deionised water by an OCA measurement system (Dataphysics, Germany) at room temperature conditions. In order to minimise the experimental error, the data obtained from these parameters were averaged by ten measurements at different random locations of each membrane sample.

2.6. Filtration experiments

The permeation properties of the membranes were characterised in terms of deionised water flux and fouling studies using a standard cross-flow filtration system, which is described in an earlier paper [11]. Flat-sheet membranes with an effective area of 70.3 cm^2 were put in the experimental setup for filtration tests. Each membrane was initially pre-pressurised at 3 bar in deionised water for 30 min before the experiments. The deionised water flux was then measured under different transmembrane pressures (ΔP) ranging from 0.5 to 3 bar at a constant flow rate of 300 L/h and 25 ºC, and calculated by Eq. (4):

$$J_W = \frac{V}{A_m \cdot \Delta t} \qquad \text{Eq. (4)}$$

where J_W is the deionised water flux ($L/m^2 \cdot h$), V is the volume of permeate water (L), A_m is the membrane effective area (m^2), and Δt is the permeation time (h).

According to Darcy's law, the intrinsic resistance of the membrane itself (R_m) was obtained from J_w using the following equation:

$$R_m = \frac{\Delta P}{\mu \cdot J_W} \qquad \text{Eq. (5)}$$

where ΔP is the transmembrane pressure (bar) and μ is the dynamic water viscosity (Pa·s).

Pore size of the high-impact polystyrene membranes was determined by water-filtration velocity method using the following equation known as the Guerout-Elford-Ferry equation, which can be used as an estimated parameter of the true pore size [11,12]:

$$r_m = \sqrt{\frac{(2.9 - 1.75 \cdot \varepsilon) \cdot 8 \mu \cdot \zeta \cdot Q_W}{\varepsilon \cdot A_m \cdot \Delta P}} \qquad \text{Eq. (6)}$$

where ζ is the membrane thickness (m) and Q_W is the water flow (m^3/s).

Separation performance of the resulting membranes was studied in terms of permeate flux (J_f, $L/m^2 \cdot h$) and rejection index (R, %) by filtration experiments of 50 mg/L HA solutions. HA concentration was selected according to previous studies about membrane characterisation [13,14]. These experiments were conducted at 25 ± 1 ºC and 2 bar. HA rejections were measured by obtaining the HA concentration in each stream using an UV-Visible spectrophotometer (Hewlett-Packard 8453) at a wavelength of 254 nm. Therefore, rejection index was calculated as follows:

$$R(\%) = \frac{C_f - C_p}{C_f} \cdot 100 \qquad \text{Eq. (7)}$$

Once the filtration experiments with HA solutions were finished, membranes were rinsed with deionised water to remove the reversible fouling from the membrane, where the rinsing flux (J_r, L/m^2·h) was measured. To evaluate the fouling-resistant capability of HIPS and HIPS-R membranes, flux recovery ratio (*FRR*) was calculated by Eq. (8):

$$FRR(\%) = \frac{J_r}{J_W} \cdot 100 \qquad \text{Eq. (8)}$$

Then, the total filtration resistance, the reversible fouling resistance (caused by the concentration polarisation phenomenon and the filtration cake) and the irreversible fouling resistance (caused by strong solute adsorption and deposition) were determined using the following equations:

$$R_T = R_m + R_{rev} + R_{irr} \qquad \text{Eq. (9)}$$

$$R_{rev} = \frac{\Delta P}{\mu \cdot J_f} - R_m - R_{irr} \qquad \text{Eq. (10)}$$

$$R_{irr} = \frac{\Delta P}{\mu \cdot J_r} - R_m \qquad \text{Eq. (11)}$$

where R_T is the total filtration resistance (obtained from the Darcy's law, which correlates this resistance with the permeate flux J and the transmembrane pressure ΔP), J_f denotes the permeate flux of the filtration of HA solutions at steady state (L/m^2·h), R_{rev} is the reversible fouling and can be defined as the flux loss in the permeate stream that can be recovered by physical cleaning, and R_{irr} is the irreversible fouling which can be defined as the flux loss in the permeate stream that can be recovered by chemical cleaning or even cannot be recovered.

3. RESULTS AND DISCUSSION

3.1. Phase diagrams for polystyrene/DMA/water ternary system

The phase-diagram for polystyrene/DMA/water ternary system is shown in Fig. 1. The curves presented in the phase-diagram describe the precipitation point of each polymer tested using DMA as a solvent and water as a non-solvent. It can be observed that both membranes (HIPS and HIPS-R membranes) presented similar tendencies, however with insignificant differences in the phase border curves (binodal curves) and the shift of the critical point. These differences may be attributable to the presence of additives in the HIPS-R matrix, which got incorporated to the plastic matrix during recycling. The changes of the binodal curve during the phase separation process directly affect the morphology of the membranes and are also heavily depending on the nature and hydrophilicity of the additives [9,15]. The incorporation of additives into the polymeric solution could cause the displacement of the binodal line toward polymer-water axis in phase diagram. These additives could enlarge the homogeneous region. Due to their hindrance effect (related to their hydrophilic properties or groups), additives could also present larger tolerance to non-solvent. Consequently, more water would be needed to precipitate the base polymer and thus leading to more delayed liquid-liquid demixing (slower precipitation) and denser structures during the membrane preparation would be obtained (thermodynamic aspect of the phase separation method) [9,16]. Additionally, the viscosity of the polymeric solution could be increased with the presence of new compounds in the polymeric solution, which would lead to a decrease in the exchange rate between solvent and non-solvent and thus resulting in a slower and longer precipitation of the casting solution (kinetic aspect of the phase separation method) [15,17]. However, the HIPS-R/DMA/water system showed a displacement of its binodal curve toward the polymer-solvent axis. This increased both the unstable gap and thermodynamic instability, which resulted in less need for non-solvent to prepare the HIPS-R membranes (Fig. 1). This rapid demixing was corroborated with the results of the measured viscosity, which are shown in Table 1. HIPS-R solutions had lower viscosity than HIPS solutions (159.9 ± 2.2 cP and 227.8 ± 2.8 cP, respectively) and therefore, more liquid HIPS-R polymeric solution showed a faster diffusion of solvent into the coagulation bath, which could favour the formation of macrovoids and results in more porous membranes [18,19]. Therefore, in view of the phase diagram for polystyrene/DMA/water ternary systems, HIPS-R membranes will show more open morphologies than HIPS membrane.

3.2. SEM/EDX analysis

SEM analysis was carried out in order to visualise the cross-sectional morphologies of both HIPS and HIPS-R membranes, which are shown in Fig. 2. It can be observed that both membranes exhibited a similar asymmetric finger-like pore structure with evident macrovoids and a thin top skin layer. This morphology matches with the typical membrane structure obtained by immersion-precipitation phase-inversion method [9]. The exchange rate or affinity between solvent (DMA) and non-solvent (deionised water) dominates this method, whereby the formation and enlargement of macrovoids (instantaneous demixing) are being favoured by the good miscibility between them [18,20]. Fig. 2 further shows that HIPS-R membrane had slightly more macrovoids and larger cavities in the sublayer than the HIPS membrane. This could be related to the presence of additives incorporated during the recycling process into its structure, which some of them could act as suppressors of macrovoids [19,21] and others could act as pore forming agents [22,23].

The element composition of the samples of both membranes was analysed using EDX spectroscopy at the same time the SEM analysis was conducted. The EDX results are shown in Table 2. As can be seen from Table 2, the presence of carbon and oxygen was observed in all the membranes, including chlorine, titanium, and silicon only in HIPS-R structures. Carbon element is present in a high percentage because it is the main element in the compounds that form the structure of the high-impact polystyrene (polystyrene and polybutadiene) and also, the thin conductive layer used to cover the samples consisted of carbon particles. In addition, oxygen was detected in both membranes. The increase in the amount of oxygen (from 1.21 ± 0.21 wt% in HIPS structures to 3.24 ± 0.22 wt% in HIPS-R membranes) may be linked to the presence of chlorine, titanium, and silicon in the post-consumer high-impact polystyrene structure, which could be related to the additives used during the recycling processes, such as reinforcing fillers, plasticisers, pigments, metal oxide nanoparticles, titanium derived coupling agents or silane coupling agents [24-26]. Some of these additives could be accumulated in the non-solvent bath after coagulation process, but others might be incorporated in the resulting membrane structure. Their presence in the structure could explain the dark colour of the HIPS-R membranes compared to the nearly white colour of HIPS membranes (not shown in the paper) [6].

3.3. FTIR-ATR

The absorbance spectra of the different membranes were recorded by Fourier transform infrared-attenuated total reflection (FTIR-ATR), which allows, together with the EDX analysis, deeper comprehension of the changes occurred in the chemical structure of the membranes. Fig. 3 presents the FTIR-ATR spectra of HIPS and HIPS-R membranes and it can be observed that both membranes had similar spectra. The absorption peaks at 2922 cm^{-1} and 2852 cm^{-1} corresponded to the C-H bond asymmetric and symmetric stretching vibrations of vinyl groups. The peaks located at 3082 cm^{-1} and 3026 cm^{-1} were attributed to aromatic C-H stretching vibrations [27]. In the same way, the absorption peaks at 1604 cm^{-1} and 1496 cm^{-1} were assigned to the aromatic C=C stretching vibrations. Compared to pure polystyrene, high-impact polysterene (as a rubber-reinformed polystyrene plastic) had enhanced strength properties due to the addition of polybutadiene (the most common rubber used), which formed graft copolymers with polystyrene [28]. The presence of polybutadiene can be demonstrated by different absorption peaks. At 1718 cm^{-1}, there was a peak attributed to the stretching vibration of C=O groups, whose presence came from polybutadiene phase and was confirmed by EDX analysis. In addition, the absorption peaks detected at 970 cm^{-1} and 910 cm^{-1} could be attributed to the out-of-plane C-H bond bending vibrations of trans-1,4 and vinyl-1,2 groups, respectively. From FTIR-ATR spectra, it can be observed that such peaks slightly decreased in the HIPS-R. Due to the overlapping styrene unit peak in polystyrene, the peak at around 754 cm^{-1} related to cis-1,4 of polybutadiene in HIPS could not be studied [8,29]. Some new absorption peaks, which were related to the presence of additives in its matrix structure, appeared in the FTIR-ATR spectrum of the HIPS-R membrane. The presence of additives containing silicon was confirmed by the long chain Si-CH_2-R groups located at around 1248 cm^{-1}, a double peak in the spectrum at 1096 cm^{-1} assigned to Si-O-C bond, and those bands related to the stretching vibrations of the Si-O bond at 880 cm^{-1} [30-32]. A weak increment of the absorption band around 910 cm^{-1} was observed. This increment was assigned to the stretching vibration of the Ti-O-Si bond [32]. Similarly, a new absorption peak is visualised at 725 cm^{-1}, which could be related to the stretching vibrations of the Ti-O-Ti bonds [33].

3.4. AFM

Atomic force microscopy (AFM) was used to record the topography of the HIPS and HIPS-R membranes over a scan size of 1 µm x 1 µm. Their three-dimensional images and surface roughness (S_a) values are shown in Table 1 and Fig. 4, respectively. The brightest area indicates the highest points of the sample whereas the dark area illustrates the valleys or pores of the surface. The surface roughness of HIPS-R membrane was slightly higher than that of HIPS membrane, where the S_a values of both membranes were 5.37 ± 1.21 nm and 4.11 ± 0.99 nm, respectively. This higher surface roughness commonly favours the accumulation of solute particles in the valleys of the membrane surface, which causes an increase in the membrane fouling resistance [34]. However, an opposite behaviour can be observed when the formation of a rougher surface is closely linked to the presence of hydrophilic additives. If the increase in roughness is caused by the accumulation of hydrophilic additives, the surface hydrophilicity of a membrane can be improved, thus reducing the interaction between the foulants and the membrane surface. Such increases in surface roughness and hydrophilicity can enhance the permeate flux and performance of a membrane and therefore, its antifouling properties [11,35].

3.5. TGA

Thermogravimetric analysis was performed to evaluate the thermal stability of the prepared membranes by comparing the weight reduction of each membrane sample with respect to temperature. The TGA curve of each membrane is shown in Fig. 5. It can be clearly observed that the decomposition of both polymer films occurred in a unique step, corresponding to thermal cracking of the polymer at around 430 ºC (at 429.16 ºC for HIPS membranes and 428.01 ºC for HIPS-R membranes). These results are in good agreement with those reported by Zhuang and colleagues about the thermal decomposition of high-impact polystyrene films [36]. The thermograms obtained for both membranes showed similar mass decrease with insignificant alteration. These results indicate that both membranes had similar thermal stability and minor structural differences despite the presence of additives in the recycled high-impact polystyrene. Additionally, these TGA results are in accordance with the FTIR-ATR and EDX results. The TGA results further highlighted the influence of additives whereby the onset of the fusion process for HIPS-R was delayed as opposed to the one for HIPS. Furthermore, only 0.19% of the HIPS sample was left as opposed to 2.30% of HIPS-R sample was left.

3.6. Porosity, EWC and Water contact angle

Results of porosity, EWC and water contact angle obtained for each membrane are shown in Fig. 6. Both porosity and EWC values were higher in HIPS-R membranes (52.31 ± 4.33 % and 51.78 ± 3.71%, respectively) than in HIPS membranes (47.54 ± 5.53% and 46.09 ± 4.16%, respectively). This might be mainly due to the presence of additives in the HIPS-R structure. The presence of additives in the HIPS-R polymeric solution as a consequence of the recycling process resulted in a lower viscosity and then, a more porous membranes (increasing number of pores and/or larger pore sizes in the sublayer) was obtained, which was confirmed before in previous analysis (the aforementioned SEM analysis and phase diagrams). This fact was confirmed by the calculation of the average pore radius for high-impact polystyrene membranes, which has been applied in studies about preparation of asymmetric membranes [11,37]. HIPS-R membrane showed higher average pore radius than the HIPS membrane, indicating that the former membrane was more porous than the latter one (see Table 3).

Similarly, HIPS-R membrane presented lower water contact angle (79.19 ± 4.15 º) than HIPS structures (81.78 ± 3.42 º), showing a slightly higher hydrophilic character than the HIPS membranes. However, both membranes could be considered as hydrophobic (or semi-hydrophilic) membranes (see Fig. 6). Generally, membrane hydrophilicity is higher when its contact angle is smaller. It could be comprehended that water contact angle decreased with an increasing presence of additives in their structure, which may have higher affinity for water (higher hydrophilic character) than base polymer and therefore, the resulting structure could present higher hydrophilicity [38].

3.7. Filtration experiments

Permeation flux and solute rejections are the main parameters to characterise the permselective properties and therefore, the membrane performance [39]. Filtration experiments were carried out in order to determine water permeability K and intrinsic membrane resistance (R_m) of membranes and the results are shown in Table 3. The water permeability value of HIPS-R membranes was higher than that obtained for HIPS membranes, mainly because HIPS-R membranes were more porous structures (see porosity and EWC results). Several researchers have demonstrated the influence of the material and the porosity of membranes on their water contact angle and on the deionised water flux [9,15,40,41]. There is a close relationship between surface hydrophilicity and water flux, by which stronger hydrophilic surfaces lead to higher water fluxes and thus, higher water permeability. The HIPS-R membranes showed higher water permeability than HIPS membranes, which could be also related to the low viscosity of HIPS-R solutions (as explained before in section 3.1). The viscosity of the polymeric solution directly affects the permeate flux, since low viscous polymeric solutions result in membranes with low resistance of flow through the polymer film and therefore, membranes with high permeability [17].

Fouling experiments were performed in order to study the antifouling properties of the prepared high-impact polystyrene membranes. Fig. 7 shows the permeate flux of each membrane for the HA solution as a function of time. It can be seen that both membranes showed similar performance with no significant difference during the filtration time. The flux rapidly declined during the first 30 minutes of the filtration experiment, which was caused by the fast accumulation of the retained solute particles on the surface and in the pores of the membranes. After that period, a progressive decline of the permeate flux occurred until a steady value, in which the equilibrium between the superficial attachment and detachment of foulants was reached [10,39]. Comparing the steady state fluxes obtained for each membrane at the end of the filtration experiment, the flux decline of HIPS-R membranes was lower than that obtained for HIPS membranes. The HIPS-R membranes showed a total flux loss of 56.9 % of the initial permeate flux value, whereas HIPS membranes had a final flux loss of 62.3 % of the initial permeate flux value. Due to the complexity of the fouling phenomena, the use of the resistance-in-series model to study in depth the flux decline during fouling experiments was considered [42]. For this reason, intrinsic membrane resistance (R_m), reversible resistance (R_{rev}), irreversible resistance (R_{irr}), total membrane resistance (R_T), and flux recovery ratio (*FRR*) were calculated in order to quantitatively evaluate fouling phenomena for the high-impact polystyrene membranes. The time evolution of *FRR* is displayed in Fig. 8. Results show that *FRR* values of the HIPS-R membranes was higher than those of the HIPS membranes. The higher hydrophilic character of HIPS-R membranes could cause a reduction of HA deposition on the surface or within the pores, which led to a lower fouling tendency. This fact was confirmed by the results of fouling resistances shown in Fig. 9, where HIPS-R had much lower reversible and irreversible resistance as compared to those for HIPS membranes. This lower resistance indicate that the HIPS-R membranes possessed better antifouling characteristics than the HIPS membrane. This could be related to the incorporation of additives into the polymeric solution.

The high contribution of the irreversible resistance is closely linked to the strong attachment of foulants to the membrane surface and its structure [43,44]. These foulants are not easily removable by physical cleaning and hence, a chemical cleaning is needed. The observed mean total fouling resistance (R_T) for HIPS and HIPS-R were 49 % and 42 %, respectively. Thus, it suggests that the presence of additives helped to reduce the strength of the hydrophobic interactions between HA molecules and the membrane surface. However, intrinsic membrane resistance (R_{rev}) is equally important as it constituted 38 and 42 % of the R_T for HIPS and HIPS-R membranes, respectively. The reversible resistance of both membranes presented similar values. This resistance is linked to the low strength of the attachment of foulants to the surface as well as the concentration polarisation phenomenon [44]. Notingly, the irreversible resistance could be considered as the differentiating factor between both membranes. The improvement in antifouling properties for the HIPS-R membrane can be clearly linked to the reduction of more than 22 % of the R_{irr} value compared to that obtained in the HIPS membrane. Given these results, it is safe to suggest that irreversible fouling can be minimised to satisfactory levels by using membranes through phase inversion from post-consumer high-impact polystyrene in low-pressure driven membrane filtration processes.

Finally, the solute rejection of each membrane is displayed in Fig. 10. It can be observed that the HA rejection for HIPS-R membranes was slightly improved as a consequence of the presence of additives in the polymeric structure. These results are in agreement with the observed improvement in previous parameters, including porosity, hydrophilicity, surface roughness and water permeability. As was explained before, previous research articles reported that there is a strong relationship between porosity and water permeability [9,45]. The presence of additives favoured the formation of a more porous membrane with a thinner skin layer, which led to a decline in the intrinsic membrane resistance and thus higher water permeability. The higher porosity together with a higher surface roughness and a lower water contact angle could result in an improvement in hydrophilicity [41,46]. The increasing trend observed in all these parameters (porosity, hydrophilicity, roughness and water permeability) for HIPS-R membranes could play an important role in the improvement of their HA rejection index, especially the membrane hydrophilicity which inhibits interactions between the membrane surface and the organic solutes [9,41].

4. CONCLUSIONS

Recycled plastic waste can be considered as an economical and environmental alternative for preparing low-pressure membranes by phase-inversion method. Virgin commercial high-impact polystyrene and post-consumer recycled high-impact polystyrene were separately used as base polymers to prepare polymeric membranes, which were subsequently compared in different characterisation tests and filtration experiments. Post-consumer high-impact membranes showed an asymmetric structure similar to that obtained for virgin commercial high-impact polystyrene membranes but with slightly higher porosity and equilibrium water content. The analysis of the thermal stability revealed that the onset of fusion process for post-consumer high-impact polystyrene membranes started after the onset of the fusion process for commercial high-impact polystyrene membranes. This might be caused by the presence of metallic and organometallic additives, which was confirmed by the FTIR-ATR and EDX results. The incorporation of different additives during the recycling process is fundamental to provide new functional properties to the polymer as well as to strengthen the expected characteristics of the original one. The additives made the membranes to become more hydrophilic, which was observed in the lower water contact angle of the recycled plastic waste membranes. Their low viscosity and high water permeability confirmed this statement. Moreover, irreversible resistance was successfully minimised and the humic acid rejection was improved in the post-consumer high-impact polystyrene membranes. This indicates that these more hydrophilic membranes had better antifouling properties. Finally, the results of the post-consumer recycled high-impact polystyrene membranes suggested that they could provide a sustainable and environmental alternative when implemented in low-pressure membrane separation processes (microfiltration and ultrafiltration).

5. ACKNOWLEDGEMENTS

The authors of this work wish to gratefully acknowledge Acteco S.L. (Spain) and BASF Co. (Germany) for supplying HIPS-R and HIPS, respectively. We also wish to thank the Center for Biomaterials and Tissue Engineeering (CBIT) for assisting with both TGA and contact angle measurements. We also wish to thank the Interuniversity Research Institute for Molecular Recognition and Technological Development (IDM) which assisted us with FTIR-ATR measurements.

6. REFERENCES

[1] F.R. Rijsberman, Water scarcity: Fact or fiction?, Agr. Water Manage. 80 (2006) 5-22.

[2] J. Bundschuh, M.C. Suárez, Introduction to the numerical modelling of groundwater and geothermal systems: Fundamentals of Mass, Energy and Solute Transport in Poroelastic Rocks (2010), Taylor and Francis Group, CRC Press, London (UK).

[3] J. Liu, Q. Liu, H. Yang, Assessing water scarcity by simultaneously considering environmental flow requirements, water quantity, and water quality, Ecol. Indic. 60 (2016) 434-441.

[4]M.C. Branco, P.D. Henriques, The political economy of the human right to water, Review of Radical Political Economics 42(2) (2010) 142-155.

[5] H. Yuan, Z. He, Integrating membrane filtration into bioelectrochemical systems as next generation energy-efficient wastewater treatment technologies for water reclamation: a review, Bioresource Technol. 195 (2015) 202-209.

[6] R. Stein, Chapter 10: Polymers, Recycling in: R.A. Meyers (Eds), Encyclopedia of Physical Science and Technology: Polymers (3rd edition), 2013, pp. 745-750.

[7] Y. Zare, Recent progress on preparation and properties of nanocomposites from recycled polymers: a review, Waste Manage. 33 (2013) 598-604.

[8] F. Vilaplana, A. Ribes-Greus, S. Karlsson, Analytical strategies for the quality assessment of recycled high-impact polystyrene: a combination of thermal analysis, vibrational spectroscopy, and chromatography, Anal. Chim. Acta 604 (2007) 18-28.

[9] J. García-Ivars, M.I. Iborra-Clar, M.I. Alcaina-Miranda, B. Van der Bruggen, Comparison between hydrophilic and hydrophobic metal nanoparticles on the phase separation phenomena during formation of asymmetric polyethersulphone membranes, J. Membr. Sci. 493 (2015) 709-722.

[10] M. Mulder, Basic Principles of Membrane Technology (2nd edition), Kluwer Academic Publishers, Springer, Dordrecht, The Netherlands, 1996.

[11] J. García-Ivars, M.I. Alcaina-Miranda, M.I. Iborra-Clar, J.A. Mendoza-Roca, L. Pastor-Alcañiz, Enhancement in hydrophilicity of different polymer phase-inversion ultrafiltration membranes by introducing PEG/Al_2O_3 nanoparticles, Sep. Purif. Technol. 128 (2014) 45-57.

[12] G. Wu, S. Gan, L. Cui, Y. Xu, Preparation and characterization of PES/TiO_2 composite membranes, Appl. Sur. Sci. 254 (2008) 7080-7086.

[13] A.R. Costa, M.N. de Pinho, Effect of membrane pore size and solution chemistry on the ultrafiltration of humic substances solutions, J. Membr. Sci. 255 (2005) 49-56.

[14] J. Lowe, Md.M. Hossain, Application of ultrafiltration membranes for removal of humic acid from drinking water, Desalination 218 (2008) 343-354.

[15] S. Mohsenpour, A. Safekordi, M. Tavakolmoghadam, F. Rekabdar, M. Hemmati, Comparison of the membrane morphology based on the phase diagram using PVP as an organic additive and TiO_2 as an inorganic additive, Polymer 97 (2016) 559-568.

[16] M. Sadrzadeh, S. Bhattacharjee, Rational design of phase inversion membranes by tailoring thermodynamics and kinetics of casting solution using polymer additives, J. Membr. Sci. 441 (2013) 31-44.

[17] K. Hendrix, M. Vaneynde, G. Koeckelberghs, I.F.J. Vankelecom, Synthesis of modified poly(ether ether ketone) polymer for the preparation of ultrafiltration and nanofiltration membranes via phase inversion, J. Membr. Sci. 447 (2013) 96-106.

[18] C.A. Smolders, A.J. Reuvers, R.M. Boom, I.M. Wienk, Microstructures in phase-inversion membranes. Part 1. Formation of macrovoids, J. Membr. Sci. 73 (1992) 259-275.

[19] E. Saljoughi, M. Amirilargani, T. Mohammadi, Effect of PEG additive and coagulation bath temperature on the morphology, permeability and thermal/chemical stability of asymmetric CA membranes, Desalination 262 (2010) 72-78.

[20] J. Barzin, B. Sadatnia, Correlation between macrovoid formation and the ternary phase diagram for polyethersulfone membranes prepared from two nearly similar solvents, J. Membr. Sci. 325 (2008) 92-97.

[21] B.S. Lalia, V. Kochkodan, R. Hashaikeh, N. Hilal, A review on membrane fabrication: structure, properties and performance relationship, Desalination 326 (2013) 77-95.

[22] L.L. Hwang, J.C. Chen, M.Y. Wey, The properties and filtration efficiency of activated carbon polymer composite membranes for the removal of humic acid, Desalination 313 (2013) 166-175.

[23] M.K. Sinha, M.K. Purkait, Enhancement of hydrophilicity of poly(vinylidene fluoride-co-hexafluoropropylene) (PVDF-HFP) membrane using various alcohols as nonsolvent additives, Desalination 338 (2014) 106-114.

[24] G. Burillo, R.L. Clough, T. Czvikovszky, O. Guven, A. Le Moel, W. Liu, A. Singh, J. Yang, T. Zaharescu, Polymer recycling: potential application of radiation technology, Radiat. Phys. Chem. 64 (2002) 41-51.

[25] F. Vilaplana, M. Martínez-Sanz, A. Ribes-Greus, S. Karlsson, Emission pattern of semi-volatile organic compounds from recycled styrenic polymers using headspace solid-phase microextraction gas chromatography-mass spectrometry, J. Chromatogr. A 1217 (2010) 359-367.

[26] K. Hamad, M. Kaseem, F. Dery, Recycling of waste from polymer materials: an overview of the recent works, Polym. Degrad. Stabil. 98 (2013) 2801-2812.

[27] F.D.R. Amado, M.A.S. Rodrigues, F.D.P. Morisso, A.M. Bernades, J.Z. Ferreira, C.A. Ferreira, High-impact polystyrene/polyaniline membranes for acid solution treatment by electrodialysis: preparation, evaluation, and chemical calculation, J. Colloid Interf. Sci. 320 (2008) 52-61.

[28] K. Hu, Z.K. Cui, Y. Yuan, Q. Zhuang, T. Wang, X. Liu, Z. Han, Synthesis, structure and properties of high-impact polystyrene/octavinyl polyhedral oligomeric silsesquioxane nanocomposites, Polym. Composites 37(4) (2016) 1049-1055.

[29] Y. Israeli, J. Lacoste, J. Lemaire, R.P. Singh, S. Sivaram, Photo- and thermoinitiated oxidation of high-impact polystyrene. I. Characterization by FT-IR spectroscopy, J. Polym. Sci. A1 32(3) (1994) 485-493.

[30] J.P. Matinlinna, S. Areva, L.V.J. Lassila, P.K. Vallitu, Characterization of siloxane films on titanium substrate derived from three aminosilanes, Surf. Interface Anal. 36 (2004) 1314-1322.

[31] F. Kuruyama, S. Suzuki, T. Oyamada, T. Furusawa, M. Sato, N. Suzuki, Facile method for preparing organic/inorganic hybrid capsules using amino-functional saline coupling agent in aqueous media, J. Colloid Interf. Sci. 349 (2010) 70-76.

[32] J. Dasgupta, S. Chakraborty, J. Sikder, R. Kumar, D. Pal, S. Curcio, E. Drioli, The effects of thermally stable titanium silicon oxide nanoparticles on structure and performance of cellulose acetate ultrafiltration membranes, Sep. Purif. Technol. 133 (2014) 55-68.

[33] M.S. Corobea, M. Stoenescu, M. Miculescu, V. Raditoiu, R.C. Fierascu, I. Sirbu, Z. Vuluga, S.I. Voicu, Titanium functionalizing and derivatizing for implantable materials osseointegration properties enhancing, Dig. J. Nanomater. Bios. 9(4) (2014) 1339-1347.

[34] E.M. Vrijenhoek, S. Hong, M. Elimelech, Influence of membrane surface properties on initial rate of colloidal fouling of reverse osmosis and nanofiltration membranes, J. Membr. Sci. 188 (2001) 115-128.

[35] L. Yan, Y.S. Li, C.B. Xiang, S. Xianda, Effect of nano-sized Al_2O_3-particle addition on PVDF ultrafiltration membrane performance, J. Membr. Sci. 276 (2006) 162-167.

[36] G.L. Zhuang, H.H. Tseng, M.Y. Wey, Feasibility of using waste polystyrene as a membrane material for gas separation, Chem. Eng. Res. Des. 111 (2016) 204-217.

[37] E. Yuliwati, A.F. Ismail, T. Matsuura, M.A. Kassim, M.S. Abdullah, Effect of modified PVDF hollow fiber submerged ultrafiltration membrane for refinery wastewater treatment, Desalination 283 (2011) 214-220.

[38] X. Zhang, Y. Wang, Y. Liu, J. Xu, Y. Han, X. Xu, Preparation, performances of PVDF/ZnO hybrid membranes and their applications in the removal of copper irons, Appl. Sur. Sci. 316 (2014) 333-340.

[39] R.W. Baker, Membrane Technology and Applications, (2nd edition), John Wiley & Sons Ltd., Chichester, UK, 2004.

[40] H. Susanto, M. Ulbricht, Photografted thin polymer hydrogel layers on PES ultrafiltration membranes: characterization, stability, and influence on separation performance, Langmuir 23 (2007) 7818-7830.

[41] J. Lin, R. Zhang, W. Ye, N. Jullok, A. Sotto, B. Van der Bruggen, Nano-WS_2 embedded PES membrane with improved fouling and permselectivity, J. Colloid Interf. Sci. 396 (2013) 120-128.

[42] M.J. Corbatón-Báguena, S. Álvarez-Blanco, M.C. Vincent-Vela, Fouling mechanisms of ultrafiltration membranes fouled with whey model solutions, Desalination 360 (2015) 87-96.

[43] R.H. Peiris, H. Budman, C. Moresoli, R.L. Legge, Understanding fouling behaviour of ultrafiltration membrane processes and natural water using principal component analysis of fluorescence excitation-emission matrices, J. Membr. Sci. 357 (2010) 62-72.

[44] J.M. Ochando-Pulido, G. Hodaifa, A. Martínez-Ferez, Permeate recirculation impact on concentration polarization and fouling on RO purification of olive mill wastewater, Desalination 343 (2014) 169-179.

[45] J. García-Ivars, M.I. Iborra-Clar, M.I. Alcaina-Miranda, J.A. Mendoza-Roca, L. Pastor-Alcañiz, Surface photomodification of flat-sheet PES membranes with improved antifouling properties by varying UV irradiation time and additive solution pH, Chem. Eng. J. 283 (2016) 231-242.

[46] A. Ananth, G. Arthanareeswaran, H. Wang, The influence of tetraethylorthosilicate and polyethyleneimine on the performance of polyethersulfone membranes, Desalination 287 (2012) 61-70.

7. LIST OF SYMBOLS

Variables

A_m	Effective area of the membrane (m^2)
C_f	Solute concentration in the feed stream (mg/L)
C_p	Solute concentration in the permeate stream (mg/L)
FRR	Flux recovery ratio (%)
J	Permeate flux during the filtration process ($L/m^2 \cdot h$)
J_f	Permeate flux at the end of the humic acid filtration ($L/m^2 \cdot h$)
J_r	Permeate flux during the rinsing process ($L/m^2 \cdot h$)
J_W	Permeate water flux / Deionised water flux ($L/m^2 \cdot h$)
K	Water permeability ($L/m^2 \cdot h \cdot bar$)
N	Number of points within the given area (dimensionless)
Q_W	Water flow (m^3/s)
R	Solute rejection index (%)
R_{irr}	Membrane irreversible resistance (m^{-1})
r_m	Average pore radius (m)
R_m	Membrane intrinsic resistance (m^{-1})
R_{rev}	Membrane reversible resistance (m^{-1})
R_T	Membrane total resistance (m^{-1})
S_a	Average roughness (nm)
T	Temperature (°C)
V	Total volume permeated during an experimental time interval (L)
W_D	Weight of dry membranes (g)
W_W	Weight of wet membranes (g)
Z	Height values of the surface sample (nm)
Z_{avg}	Average of the Z values of the sample (nm)

Z_i	Z value currently measured (nm)
ΔP	Transmembrane pressure (bar)
Δt	Filtration time (h)

Greek letters

ε	Membrane porosity (%)
ζ	Membrane thickness (m)
μ	Dynamic water viscosity (Pa s)
ρ_P	Density of the polymer (g cm^{-3})
ρ_W	Density of pure water at operating conditions (g cm^{-3})

Abbreviations

AFM	Atomic force microscopy
DMA	N,N-Dimethylacetamide
EDX	Energy dispersive X-ray spectroscopy
EWC	Equilibrium water content
FTIR-ATR	Fourier transform Infra-Red spectroscopy with attenuated total reflectance
HA	Humic acid
HATR	High attenuated total reflectance
HDPE	High-density polyethylene
HIPS	Commercial high-impact polystyrene
HIPS-R	Post-consumer recycled high-impact polystyrene
NIPS	Non-solvent induced phase separation
NOM	Natural organic matter

PET	Polyethylene terephthalate
PP	Polypropylene
PVC	Polyvinyl chloride
SEM	Scanning electron microscopy
TGA	Thermogravimetric analysis
UF	Ultrafiltration

Table 1. Viscosities and surface roughness (S_a) of each high-impact polystyrene membrane prepared by phase-inversion method.

Sample	Viscosity (cP)	S_a (nm)
HIPS	227.8 ± 2.8	4.11 ± 0.99
HIPS-R	159.9 ± 2.2	5.37 ± 1.21

Table 2. EDX results of HIPS and HIPS-R membranes.

Sample	Element									
	C		O		Cl		Ti		Si	
	wt%		wt%		wt%		wt%		wt%	
HIPS	98.79	± 0.22	1.21	± 0.21	---	---	---	---	---	---
HIPS-R	96.32	± 0.25	3.24	± 0.22	0.06	± 0.02	0.33	± 0.03	0.05	± 0.02

Table 3. Average pore radius (r_m) and water permeability (K) of each high-impact polystyrene membrane prepared by phase-inversion method.

Sample	r_m (nm)	K (L/m^2·h·bar)
HIPS	29.75 ± 1.88	171.21 ± 2.62
HIPS-R	32.45 ± 1.12	180.62 ± 0.71

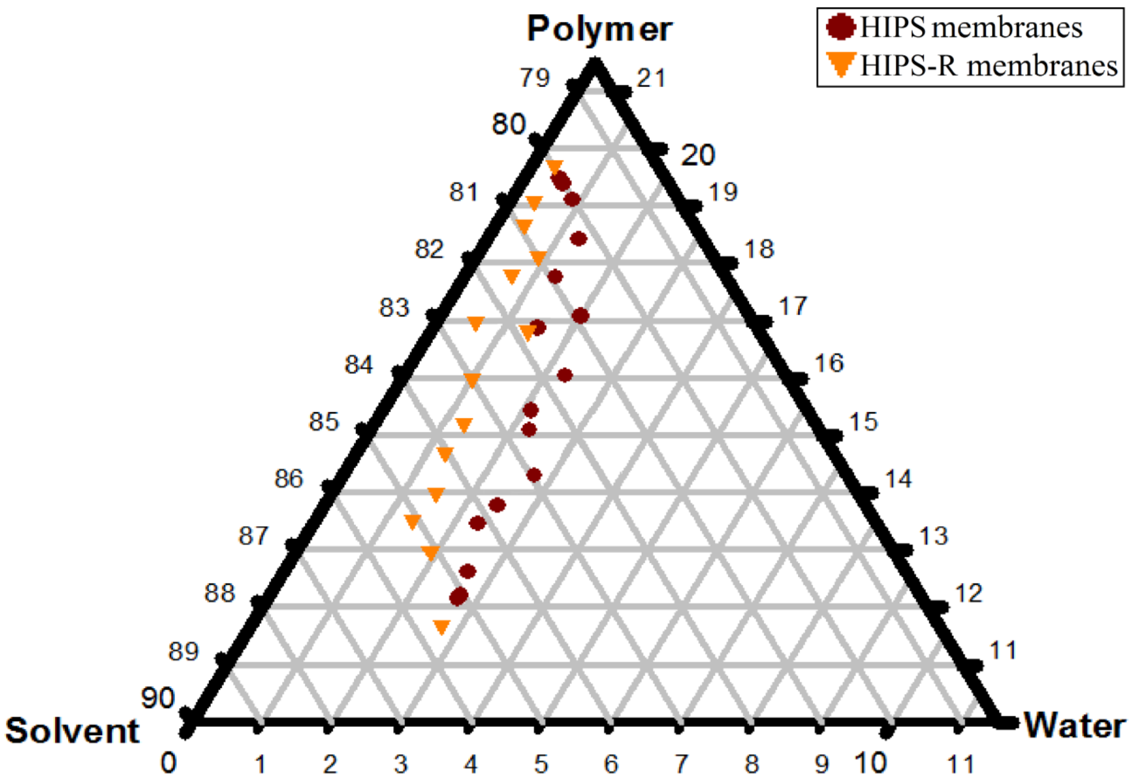

Fig. 1. Ternary phase diagram for high-impact polystyrene membranes using commercial and post-consumer high-impact polystyrene as base polymers, and NMP as a solvent constructed based on cloud point measurements by titration method at 20 º C.

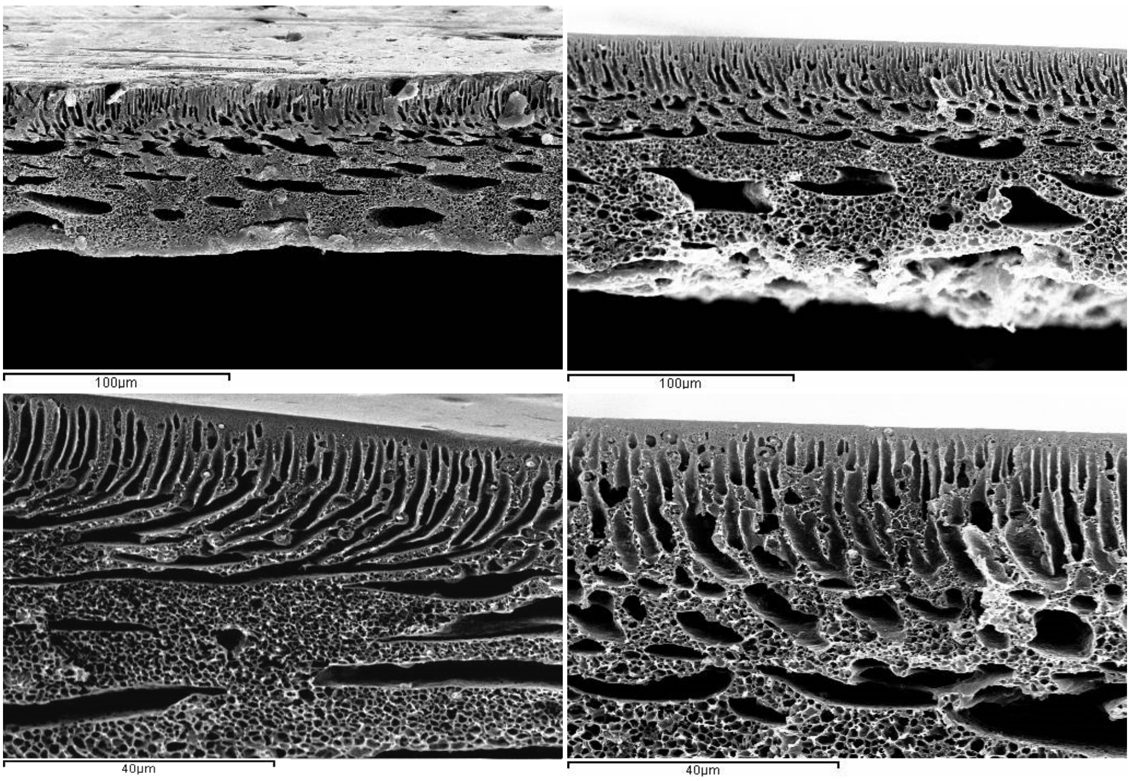

Fig. 2. SEM images of the cross-sections from HIPS (left) and HIPS-R (right) membranes.

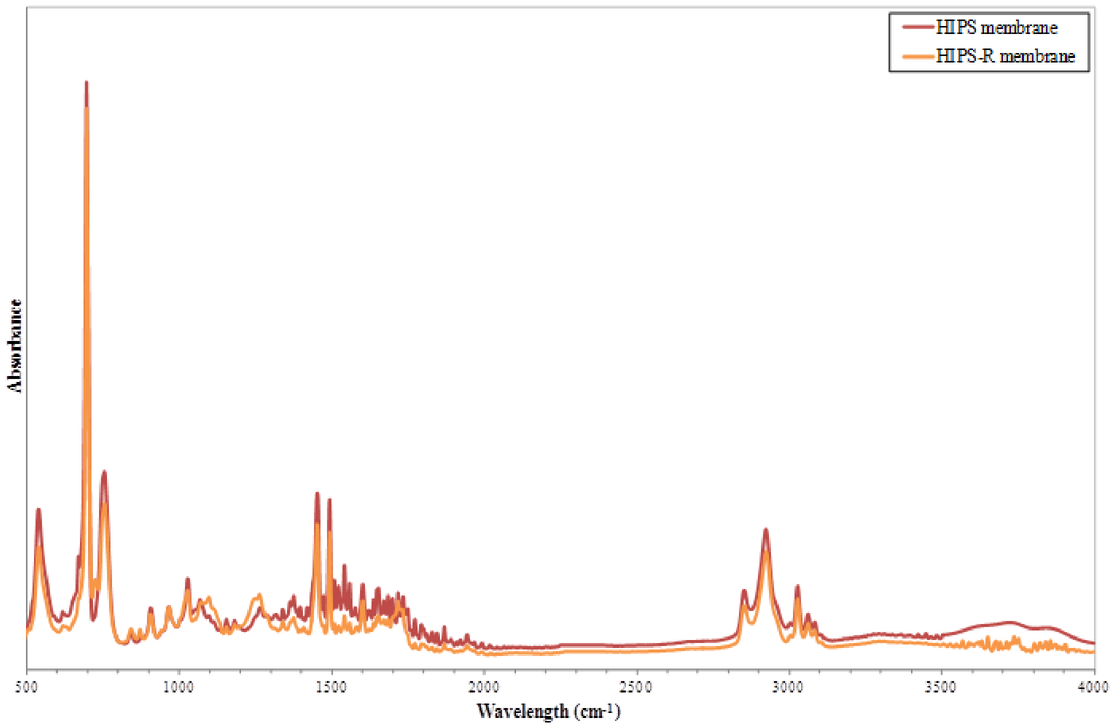

Fig. 3. FTIR-ATR spectra of the HIPS and HIPS-R membranes.

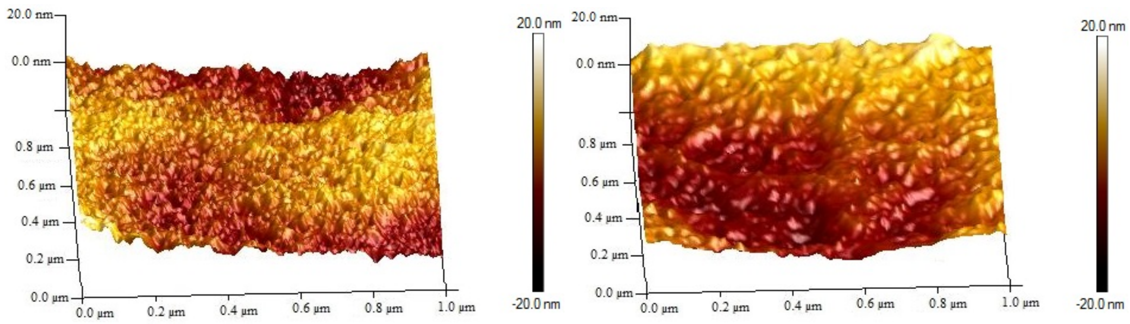

Fig. 4. Three-dimensional AFM images of HIPS (left) and HIPS-R (right) membranes.

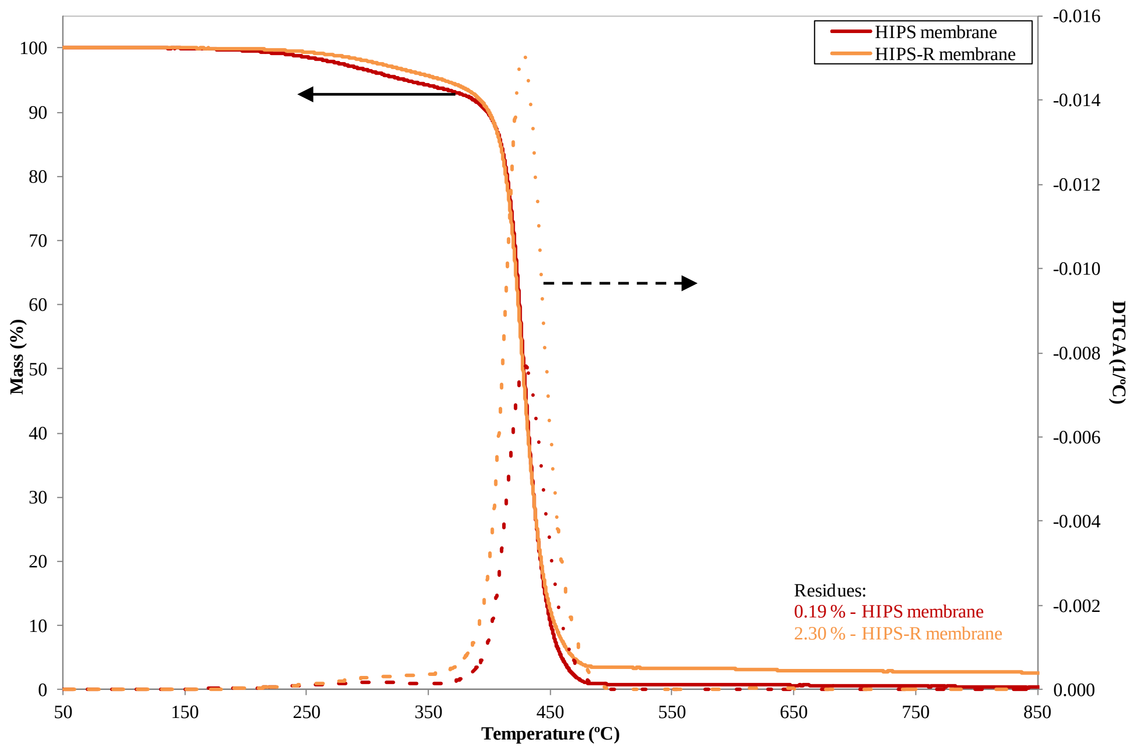

Fig. 5. Thermogravimetric analysis of HIPS and HIPS-R membranes.

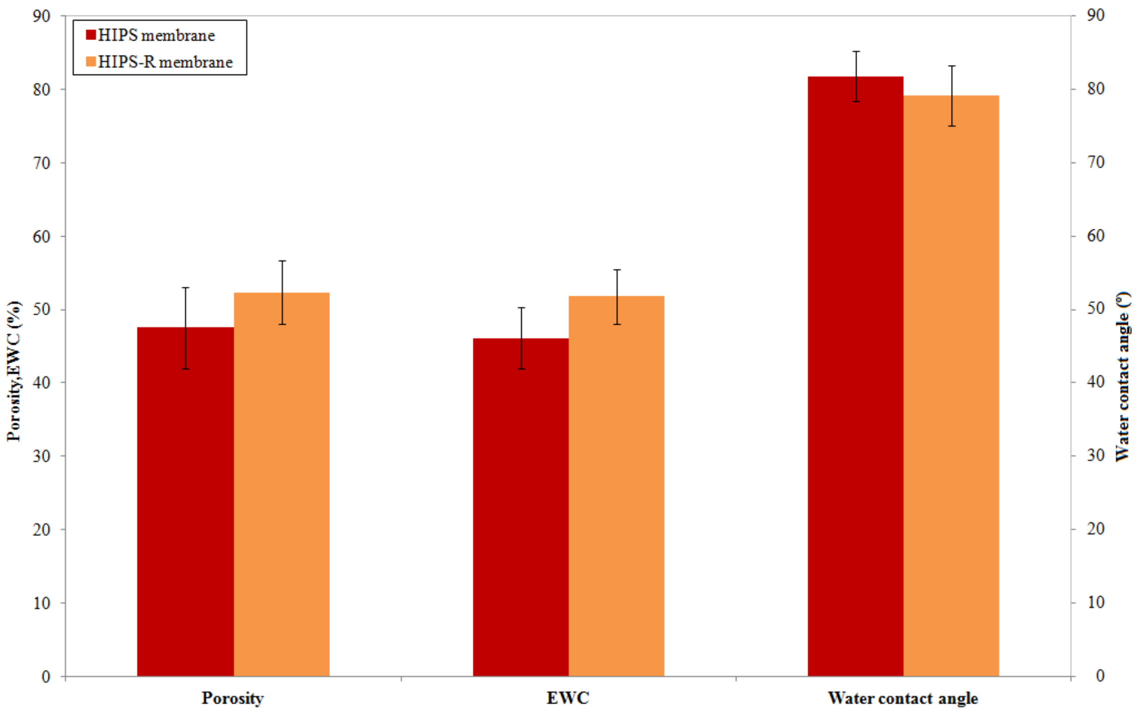

Fig. 6. Porosity, equilibrium water content (EWC) and water contact angle measurements of HIPS and HIPS-R membranes.

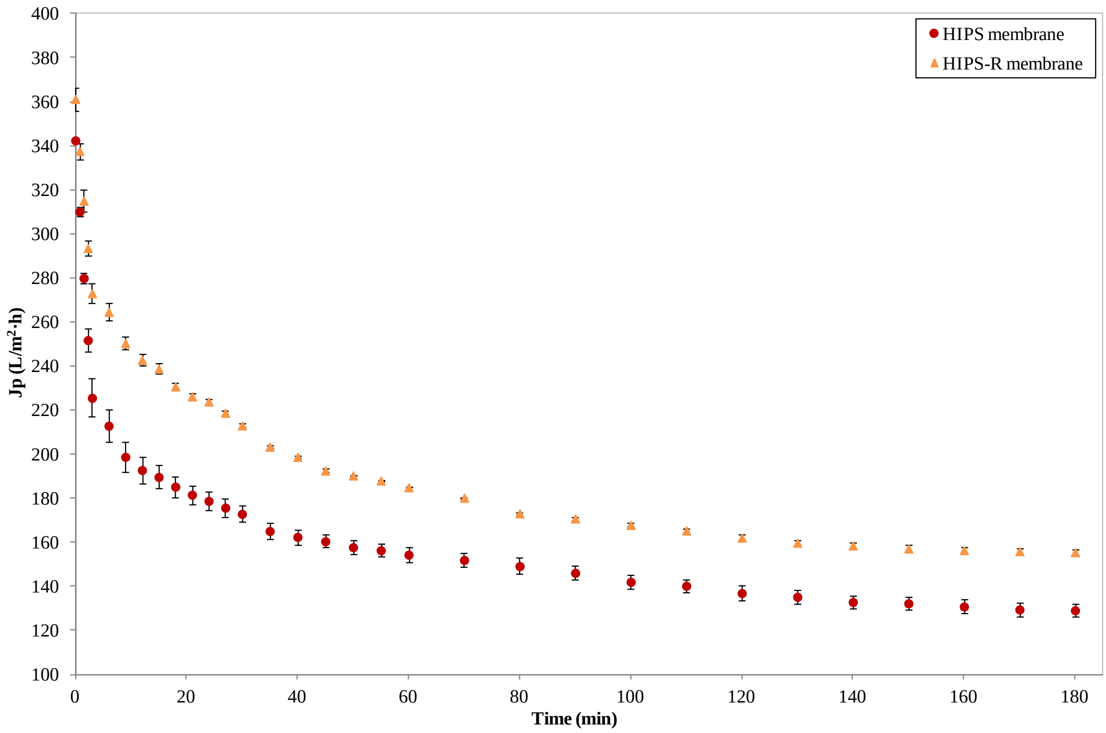

Fig. 7. Time evolution of the permeate flux of each HIPS and HIPS-R membrane using humic acid solution at a concentration of 50 mg/L, 25 ºC, 2 bar.

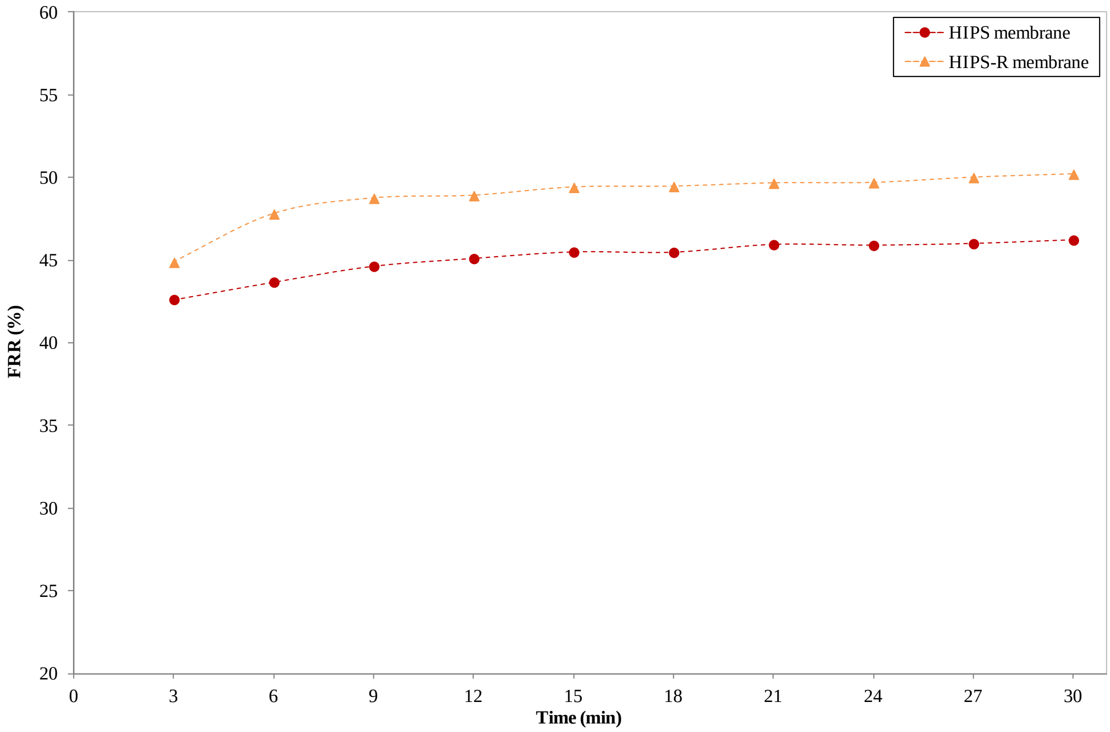

Fig. 8. Time evolution of the FRR parameter of each HIPS and HIPS-R membrane during rinsing process (300 L/h, 25 ºC, 1 bar).

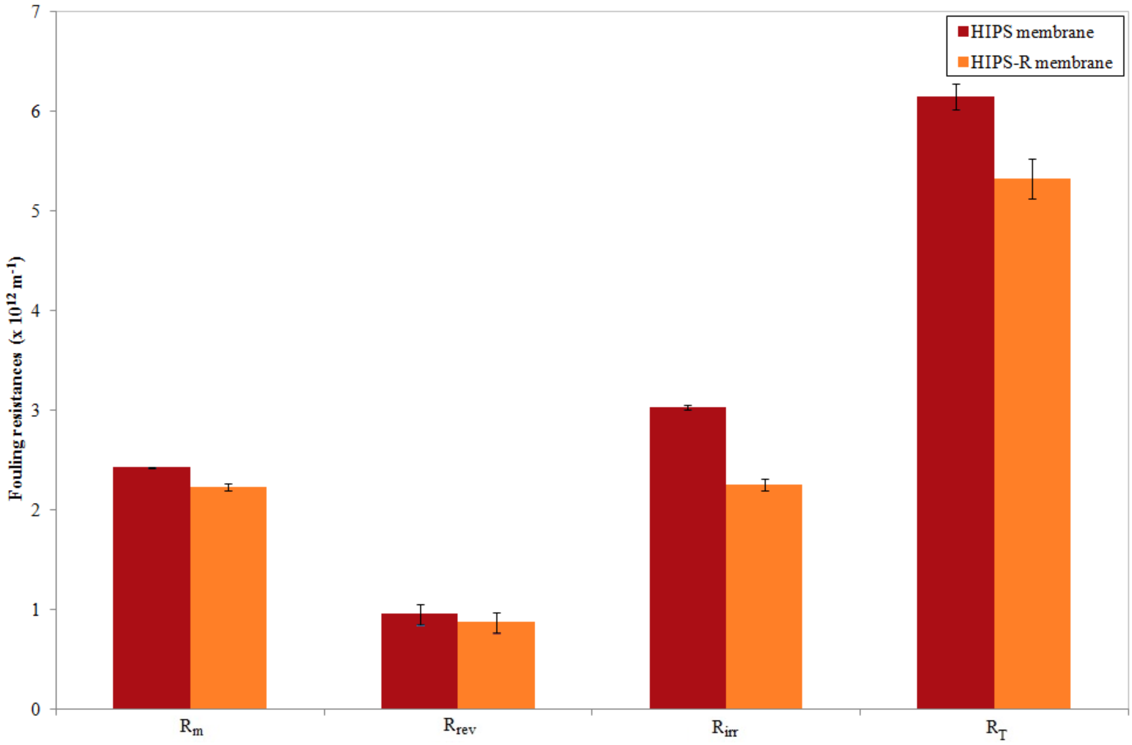

Fig. 9. Intrinsic membrane resistance (R_m), reversible fouling resistance (R_{rev}), irreversible fouling resistance (R_{irr}), and total fouling resistance (R_T) of each HIPS and HIPS-R membrane determined from filtration experiments of humic acid solution (50 mg/L, 25 ºC, 2 bar).

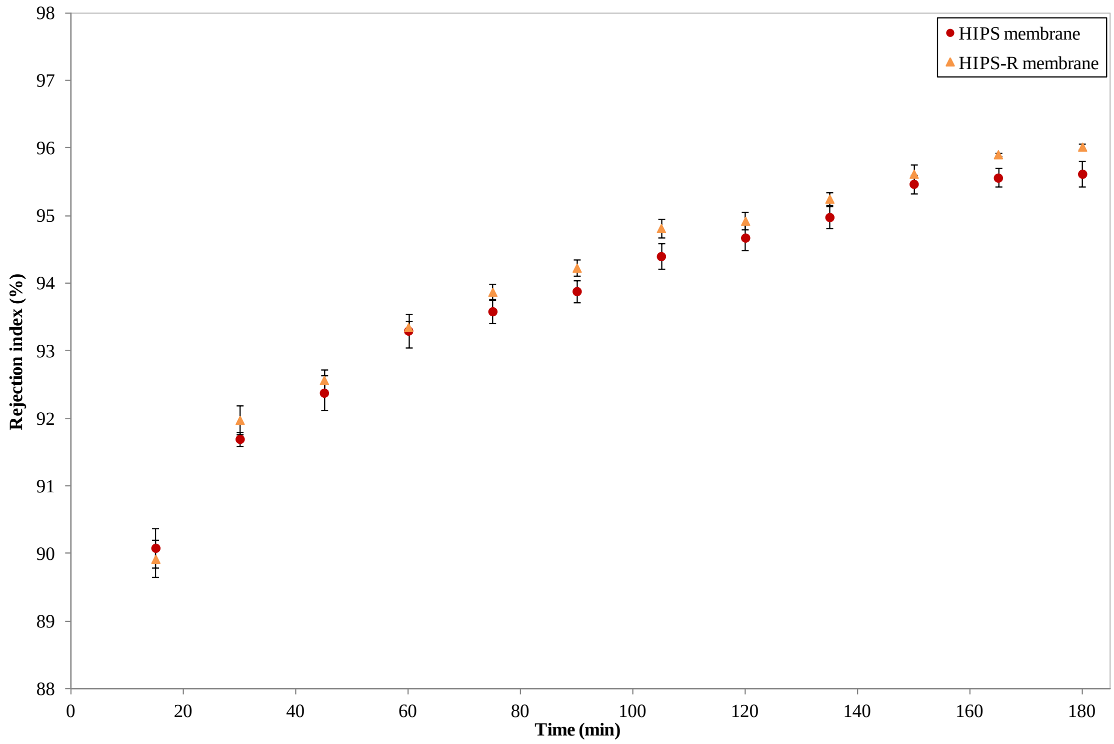

Fig. 10. Rejection index of humic acid solution (50 mg/L, 25 ºC, 2 bar) by HIPS and HIPS-R membranes.